Computational study of a weakly compressible mixing barrier in low Prandtl number, strongly stratified fluids

Richard M. McLaughlin, Hong Zhou,[a] and M. Gregory Forest
Department of Mathematics, University of North Carolina, Chapel Hill, North Carolina 27599-3250

(Received 30 December 2002; accepted 16 June 2003; published 27 August 2003)

The effects of weak compressibility in the evolution of a fluid governed by the anelastic fluid equations are explored computationally. The basis for this study is a careful determination of the role which the anelastic divergence constraint plays in the evolution of a periodic array of interacting vortices. Our numerical studies address a blocking phenomenon occurring in strongly stratified flows with small Prandtl numbers. Computationally, we first document this blocking event which strongly limits vertical mixing. This is achieved using idealized equations of fluid motion which do not excite a density perturbation and exhibits that the presence of a strong density transition layer, consistently modeled in the anelastic mass balance, may lead to a dramatic modification of vortex interactions when compared with the incompressible analog. These modifications are evidenced by the formation of a weakly compressible mixing barrier. We subsequently isolate this particular blocking phenomenon as emerging in the limit of small Prandtl number through a sequence of computational simulations of the complete anelastic fluid equations which retain a density perturbation. It is shown that a sequential reduction of the Prandtl number yields much weaker vertical mixing as evidenced by passive tracer statistics. © *2003 American Institute of Physics.* [DOI: 10.1063/1.1602695]

I. INTRODUCTION

The atmosphere is a compressible fluid admitting strong, vertical density variations over scales on the order of the atmospheric scale height (approximately 8 km in our atmosphere). Necessarily, this strong density variation, given by some mean state, $\rho(z)$, must be consistently modeled:[1] For quantified accuracy in the simulation of deep atmospheres, one may utilize a generalization of the Boussinesq approximation known as the anelastic fluid equations.[2–5] These equations suppress sound waves but retain a nonsolenoidal mass constraint, $\nabla\cdot(\rho(z)\mathbf{v})=0$, and thereby offer a compromise between the integration of the fully compressible equations (which require an *extremely* small time step), and the incompressible Boussinesq equations (which are invalid over large vertical scales, and involve the global inversion of elliptic operators to reconstruct the pressure). There is an accepted wisdom in the fluid dynamics community that the primary phenomenological details are captured within the Boussinesq limit of the anelastic equations, and the main purpose of retaining effects of density variation beyond the standard Boussinesq approximation is purely for obtaining a more quantitatively accurate approximation. In the following, we will present a model study probing the extent to which *phenomena* may be the direct result of a variable density mass balance such as that retained in the anelastic, as opposed to Boussinesq approximation.

Certainly, an interesting class of problems which has not received great attention in the literature arises in an attempt to understand how such a nontrivial anelastic mass constraint may lead to modified dynamics and mixing properties relative to the analogous incompressible system. Computational studies[3,6–8] have successfully demonstrated that anelastic effects are important in obtaining *quantitatively* correct simulations for typical large scale atmospheric density profiles, but have not elucidated precisely how variation in the density profile may alter the predictions.

In the context of scalar mixing, McLaughlin and Forest[9] have demonstrated using methods of homogenized averaging that idealized (small scale, weakly compressible) anelastic flows involving a structured background density field yield quite different effective mixing properties than their incompressible counterpart. Specifically, the presence of a density transition layer, such as that found in many boundary layers, may lead to anisotropic effective diffusion arising in the form of local regions of trapped and focused contaminants near the transition height. Motivated by this work, our purpose in this article is to explore, through a careful computational study of an idealized set of anelastic fluid equations, new phenomena associated with structure modeled in the mean state density profile. To make such a determination, we will first idealize to a model which focuses upon dynamic effects directly attributable to the variable density mass balance.

To extract the precise dynamic effects originating from the mean state, we present a set of weakly compressible fluid equations which retain a fixed, variable coefficient, prescribed mean state density profile, and a consistent, nontrivial mass balance, while neglecting all effects of buoyancy. We present formal arguments to show that these idealized equations yield limiting dynamics for strongly stratified situations in which inertial effects dominate effects

[a]Present address: Department of Applied Mathematics and Statistics, University of California, Santa Cruz, CA 95064.

of buoyancy. Examples of such scenarios may include low Prandtl number fluids, flow in microgravity, or high Froude number flow: any driven flow in which the density perturbation relaxes immediately to a nontrivial mean state density field which is maintained by external sourcing. The equations we study model an inertially dominated system in the presence of strong *maintained* density variation and consequently, our study delineates phenomena associated with gravity waves and buoyancy instability from behavior arising through the anelastic mass balance. The system is also interesting as a variable-coefficient generalization of incompressible Navier–Stokes, with physically motivated coefficients.

Through computational simulation of these idealized equations, we exhibit an intriguing *compressible mixing barrier*. This is established by a direct comparison between the dynamics of a purely incompressible, constant density fluid flow with that of the anelastic equations for a velocity field initialized as a periodic array of vortices. In the absence of strong density transition such as associated with structureless (exponential or linear) mean state profiles, there is little phenomenological difference between the vortex dynamics of the anelastic and incompressible models. However, the presence of density transition as modeled in the mean state density profile is seen to greatly change the dynamic interaction of these vortices as compared with the incompressible system, and leads to a *mixing barrier* which effectively separates the fluid system into two distinct regimes. This behavior is distinguished from the more typical blocking behavior occurring in *low* Froude number flow in that gravity plays no role in the dynamics studied here. To document the validity of the formal arguments we use to justify the simplified model anelastic system, we reintroduce gravity and explore how the influence of a density perturbation modifies the dynamics. To this end, we simulate this complete anelastic system for four different Prandtl numbers (Pr=10,1,0.1,0.01) and exhibit how this particular blocking event arises in the low Prandtl number limit. We remark that this phenomenon is similar in spirit with existing compressible passive scalar studies[9,10] designed to assess the role of a structured density profile in modifying vertical transport; however, the present case involves fully nonlinear, dynamic simulations.

II. ANELASTIC EQUATIONS

An important development in the study of atmospheric fluid flow was the recognition that for deep convection, effects of fluid compressibility should have some quantitative affect upon the dynamics; however, sound propagation could be neglected through the consideration of anelastic, ''soundproof'' fluid equations.[2,5] There have been numerous studies proposing differing modeling approaches as to the precise form of the equations,[1,3–6,11,12] however the essential distinction from the more familiar Boussinesq equations common to all of these studies is the retention of some mean state variable density profile, $\rho(z)$, varying in the vertical, and the associated *consistent* mass balance $\nabla\cdot(\rho(z)\mathbf{u})=0$. If the mean state density is taken to be exactly a constant, the equations reduce to the standard Boussinesq equations for thermal convection in a thin layer. Of course, the mean state density in the atmosphere admits strong variation, especially over large vertical scales, and consequently the Boussinesq equations do not offer a valid model to assess atmospheric phenomena. Nonetheless, the methodology employed to justify these weakly compressible anelastic models is low Mach number theory, which generally necessitates the consideration of a nontrivial fluid divergence constraint.[11,13]

The mean state profile most typically considered is that designed to account for the gravitational compression of an ideal gas under its own weight. These profiles are commonly structureless exponentials, or power laws (depending upon the precise thermodynamic assumptions), which vary slowly in the vertical. A scale for these profiles may be defined as the height over which the associated hydrostatic pressure distribution drops from its surface value by a factor of e (typically around 8 km for the Earth's atmosphere).[14] However, it should be observed that these profiles arise in the most elementary situations, and do not in any way attempt to account for the multitudes of other possible forces which may give rise to vertical atmospheric density variation (such as mechanisms producing stable boundary layers in the lower atmosphere, as well as the radiative mechanisms responsible with the change of stability occurring around the tropopause).

To begin to assess potential phenomena associated with a structured mean state density profile, we consider the following system of weakly compressible fluid equations governing the velocity field, $\mathbf{u}$:

$$\mathbf{u}_t+(\mathbf{u}\cdot\nabla)\mathbf{u}=-\frac{1}{\rho(z)}\nabla P+\frac{\mu}{\rho(z)}\Delta\mathbf{u}+\frac{\mu+\lambda}{\rho(z)}\nabla(\nabla\cdot\mathbf{u}), \tag{1}$$

$$\nabla\cdot(\rho(z)\mathbf{u})=0. \tag{2}$$

Here, $\mathbf{u}$ is the fluid velocity vector, μ, λ denote the respective first and second coefficients of viscosity, and $\rho(z)$ denotes the *prescribed*, fixed density profile. These equations clearly represent a modified Navier–Stokes system with a prescribed variable coefficient.

A few remarks are in order regarding the model system (1) and (2). First, we do not describe the mechanisms which give rise to the fixed density profile, but instead focus upon phenomenological behavior arising from the incorporation of structure into this mean state. Second, we do not at present allow for a density perturbation (see the following for direct comparison to dynamics which do). Of course, the density perturbation comprises an essential ingredient for the evolution of the atmospheric system; however, our purpose here is to isolate phenomena originating solely through structure incorporated into the mean state density field as opposed to that associated with buoyancy stability and instability. These equations yield an analogous system to that of the ideal, incompressible, constant-density, Navier–Stokes equations, only for flow moving in the presence of a prescribed density profile. As such, this system may be viewed as governing the transient behavior associated with a stirred, low Prandtl (or high Froude) number fluid with maintained mean-state, vertical density structure (or essentially the same: fluid motion at low gravity). This weakly compressible system idealizes

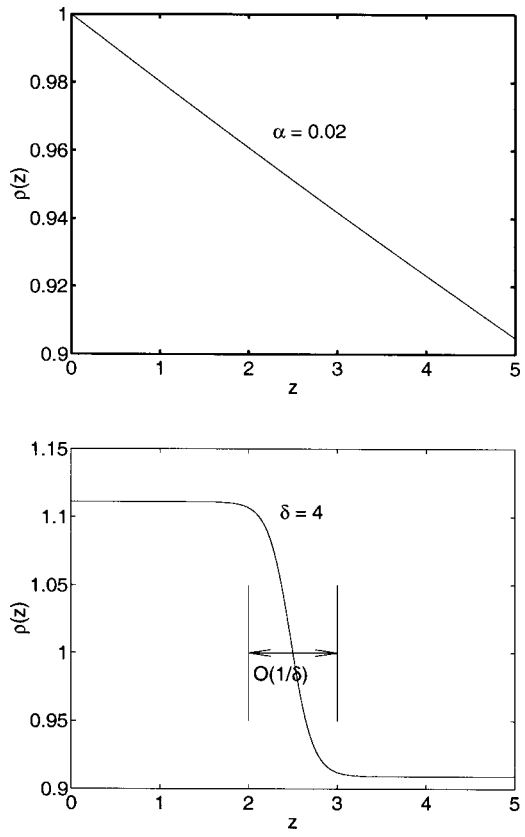

FIG. 1. The variable density profiles, $\rho(z)$, for the structureless (4) and structured (5) simulations.

fluid motion where the density of fluid parcels is assumed to immediately relax to the prescribed mean state profile. We will in the following below that (1) and (2) indeed capture phenomena to be distinguished and attributable to the anelastic mass balance by (a) presenting a formal scale analysis identifying the emergence of this system in the limit of small Prandtl number, and (b) documenting that the blocking phenomena documented in the following desists for increasing Prandtl number through direct numerical comparison between a complete set of anelastic equations involving an evolving density perturbation. Third, we emphasize that the phenomena observed in the simulations presented in the following do not depend strongly upon the precise form of the viscous stress tensor. The numerical method we employ requires some viscosity to be stable, and as such, we utilize the consistent stress tensor associated with the compressible flow in Eqs. (1) and (2).

To address phenomena associated with a structured mean density field, we will consider $\rho(z)$ to be a given function of altitude that represents various forms of atmospheric stratification, the first corresponding to a structureless mean state, the second corresponding to a density transition layer. We consider three cases here.

Case 1:

$$\rho(z) \equiv \text{constant}. \tag{3}$$

Case 2:

$$\rho^{-1}(z) = e^{\alpha z}, \tag{4}$$

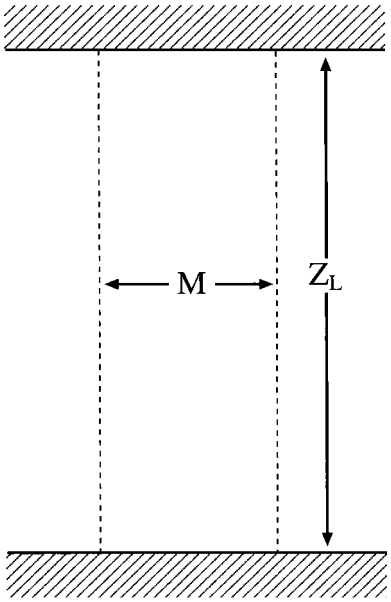

FIG. 2. A diagram of the flow region.

with α a constant parameter.

Case 3:

$$\rho^{-1}(z) = 1 + \epsilon \tanh[\,\delta(z - z_L/2)\,], \tag{5}$$

where ϵ, δ, z_L are constants, Z_L is the width of the channel, ϵ sets the amplitude of the density change across the layer, and δ sets the layer thickness.

Figure 1 documents two different density profiles for cases with $\alpha = 0.02$ in the exponential case, and $\epsilon = 0.1$, $\delta = 4$ for the transition layer.

We note that such density transitions are common occurrences in many atmospheric boundary layers and in thermoclines in lakes and oceans. We view such hyperbolic tangent density profiles as simplified cartoons representing such scenarios.

For the computational simulations we adopt channel flow boundary conditions. That is, we consider two-dimensional motions vertically limited by two parallel fixed boundaries separated by the distance Z_L (see Fig. 2). We assume no-slip boundary conditions on the vertical channel walls, and apply periodic boundary conditions in the horizontal direction, over a horizontal width, M.

The initial conditions we study are selected to produce nontrivial vortex dynamics. The velocity field is initialized as a standard cellular flow (which is an exact solution of the two-dimensional inviscid, incompressible Euler equations) plus a shear flow designed to ensure the no-slip conditions at the top and bottom walls. We additionally normalize this initial field by the mean-state density profile to correctly respect the nontrivial flow divergence constraint (2):

$$u_0(x,y) = \frac{\cos(2\pi x)\sin(2\pi y)}{\rho(z)}, \qquad v_0(x,y) = \frac{\sin(2\pi x)[1 - \cos(2\pi y)]}{\rho(z)}. \tag{6}$$

By adjusting the channel width, M, and height, Z_L, the scale of this initial array of vortices will be changed relative to the box size and to the scale of the background density profile. We further comment that while such no-slip boundary conditions may not be common for atmospheric systems (especially the top no-slip condition), we utilize these boundary conditions simply to initiate interesting vortex dynamics. The bulk of the subsequent evolution which will yield the compressible mixing barrier occurs in the interior far from the walls.

III. NONDIMENSIONAL SCALINGS, AND THE LOW PRANDTL NUMBER REDUCTION

We will begin by considering the complete anelastic fluid equations, with idealized thermodynamics, and assess the scales which give rise to the simplified zero gravity equations outlined in Sec. II. We will not pursue the more general problem of beginning with the fully compressible Navier–Stokes equation, and the associated low Mach number theory necessary to obtain these starting equations which are a generalization of the familiar Boussinesq equations; such calculations are outlined in the work of Almgren.[11] To this end, we consider the following set of coupled nonlinear partial differential equations for unknowns, $(\mathbf{u}, P, \rho')$, the respective fluid flow vector, pressure, and density perturbation:

$$\frac{\partial \mathbf{u}}{\partial t} + (\mathbf{u}\cdot\nabla)\mathbf{u} = -\frac{1}{\rho(z)}\nabla P + \frac{\mu}{\rho(z)}\Delta\mathbf{u} - \frac{\rho' g}{\rho(z)}\hat{\mathbf{z}}, \tag{7}$$

$$\nabla\cdot(\rho(z)\mathbf{u}) = 0, \tag{8}$$

$$\frac{\partial \rho'}{\partial t} + (\mathbf{u}\cdot\nabla)\rho' = \kappa\Delta\rho' - \frac{d\rho(z)}{dz}\mathbf{u}\cdot\hat{\mathbf{z}} + Q_c. \tag{9}$$

Here, we have suppressed effects of second viscosity coefficients for brevity in exposition. The full density field is $\rho(z)+\rho'$, and g denotes the gravitational acceleration. Lastly, we have placed all effects of condensational heating into the representative term, Q_c. We will not focus upon important effects of condensational heating and other phase change phenomena in the present article, but merely include this term to document that under a suitable, well-defined scaling, such effects may be neglected. We note that these equations are a generalization of the Boussinesq equations which allow for motion against a fixed, but variable coefficient background. In some forms of the anelastic equations, this background is allowed to itself vary dynamically, and can be made to satisfy reasonable thermodynamic equations of state.[11] This is the most consistent and thermodynamically reasonable approach to such systems, however, for simplicity in the present discussion, we assume that this background density variability is a steady, fixed function of the vertical coordinate.

There are a variety of different nondimensionalizations which may be employed, and we choose one with length and time scales given by the viscosity and gravity. To this end, define length and time scales through

$$\nu = \frac{\mu}{\rho_0}, \tag{10}$$

$$L = \left(\frac{\nu^2}{g}\right)^{1/3}, \tag{11}$$

$$T = \left(\frac{\nu}{g^2}\right)^{1/3}, \tag{12}$$

$$V = \frac{L}{T} = (g\nu)^{1/3}. \tag{13}$$

Here, ρ_0 is a reference (constant) density, and so ν denotes the usual kinematic viscosity of the fluid. Taking the Prandtl number to be the ratio of the kinematic viscosity and (thermal) diffusivity, $\mathrm{Pr} = \nu/\kappa$, the general anelastic equations presented above may be readily nondimensionalized yielding:

$$\overline{\rho}(z) = \rho(Lz), \tag{14}$$

$$\frac{\partial \mathbf{u}}{\partial t} + (\mathbf{u}\cdot\nabla)\mathbf{u} = -\frac{1}{\overline{\rho}(z)}\nabla P + \frac{1}{\overline{\rho}(z)}\Delta\mathbf{u} - \frac{\rho'}{\overline{\rho}(z)}\hat{\mathbf{z}}, \tag{15}$$

$$\nabla\cdot(\overline{\rho}(z)\mathbf{u}) = 0, \tag{16}$$

$$\frac{\partial \rho'}{\partial t} + (\mathbf{u}\cdot\nabla)\rho' = \frac{1}{\mathrm{Pr}}\Delta\rho' - \frac{d\overline{\rho}(z)}{dz}\mathbf{u}\cdot\hat{\mathbf{z}} + \frac{1}{\rho_0}\left(\frac{\nu}{g^2}\right)^{1/3} Q_c. \tag{17}$$

We note that with this nondimensionalization, allowing for a general, variable coefficient background density function, $\overline{\rho}(z)$, the usual Rayleigh number is not immediately observed, as in the familiar case with a linear background density profile.

The idealized, simplified form (1) and (2) of the anelastic equations is now readily obtained in the limit of small Prandtl number, provided the condensational heating effects satisfy

$$\frac{1}{\rho_0}\left(\frac{\nu}{g^2}\right)^{1/3} Q_c \ll 1.$$

Without doubt, in situations such as dry convection this last inequality may be satisfied, however, for situations involving moist convection, the underlying physics must be accounted for.

In the following sections, we will document a blocking event originating directly from the anelastic mass balance and directly captured by the simplified evolution equations (1) and (2). We accomplish this through a detailed comparison between (1) and (2), the incompressible fluid equations, and the complete anelastic system, through a sequence of simulations in which the Prandtl number is varied.

IV. THE NUMERICAL SCHEMES

Our simulations utilize a modification of the projection method introduced by Chorin.[15] We remark that it is convenient to change fluid flow variables to arrive at a modified *incompressible* flow system which may be readily simulated utilizing Hodge decomposition.[16] To this end, introduce

$$h = \frac{1}{\rho}, \quad \mathbf{u} = h\mathbf{v}, \tag{18}$$

where $\mathbf{v}=(v_1,v_2)^t$. Then Eqs. (1) and (2) become

$$\mathbf{v}_t+h(z)\mathbf{v}\cdot\nabla\mathbf{v}+h'(z)\begin{pmatrix} v_1v_2 \\ v_2^2\end{pmatrix} = -\nabla P+\mu\Delta(h(z)\mathbf{v})+(\lambda+\mu) \times\begin{pmatrix} h'(z)\dfrac{\partial v_2}{\partial x} \\ h'(z)\dfrac{\partial v_2}{\partial z}+h''(z)v_2\end{pmatrix}, \tag{19}$$

$$\nabla\cdot\mathbf{v}=0. \tag{20}$$

Let $\omega=\nabla\times\mathbf{v}$ be the vorticity. To gain some intuition about this system, suppose we ignore the viscosity term. Taking the curl of (19) and with the help of (20), one finds

$$\frac{\partial\omega}{\partial t}+h(\mathbf{v}\cdot\nabla)\omega=v_2(h''v_1-2h'\omega). \tag{21}$$

In the limiting case of constant background density, this system reduces to the familiar two-dimensional vorticity transport equation. However, nonconstant background density profiles clearly involve a modified vorticity equation. In the following, we will computationally examine the ensuing differences in evolution.

We use the projection method,[15] together with fast Fourier transform (FFT), to solve Eqs. (19) and (20) where $\lambda+\mu=0$. The outline of our numerical methods to solve the weakly compressible equations (19) and (20) in a semiperiodic region is as follows.

(1) Find U^* which satisfies

$$\frac{U^*-U^n}{\Delta t}=-\nabla p^{n-1/2}-h(z)[(U\cdot\nabla)U]^n+\frac{\mu}{h(z)}\frac{\Delta h(z)(U^n+U^*)}{2}. \tag{22}$$

(2) Project U^* to obtain U^{n+1}:

$$U^{n+1}=\mathbf{P}(U^*). \tag{23}$$

More specifically, solve

$$\Delta\phi=DU^*, \tag{24}$$

and then set

$$U^{n+1}=U^*-G\phi, \tag{25}$$

where D and G are discrete divergence and gradient operators.

(3) Update the pressure gradient according to

$$\nabla p^{n+1/2}=\nabla p^{n-1/2}+\frac{1}{\Delta t}(I-\mathbf{P})U^*. \tag{26}$$

In the spatial direction, a finite difference method is used. To solve the elliptic equation (24) numerically, we use FFT with the periodic boundary conditions for ϕ in the horizontal direction and the Neumann boundary condition at the walls. In the time direction, a predictor-corrector method (Heun's method) is employed on U and ∇p. We note that the convergence of this algorithm depends strongly upon the incorporation of an explicit, nonzero viscosity. We utilize a small, nonzero viscosity in the simulations described in the following (precise values documented in Sec. V), and emphasize that the observed behavior is not directly a result of this viscosity.

To solve the system (7)–(9) numerically, we take advantage of (18) and convert the system into the following form:

$$\mathbf{v}_t+h(z)\mathbf{v}\cdot\nabla\mathbf{v}+h'(z)\begin{bmatrix} v_1v_2 \\ v_2^2\end{bmatrix}=-\nabla P+\mu\Delta(h(z)\mathbf{v})-\rho' g\begin{bmatrix}0\\1\end{bmatrix}, \tag{27}$$

$$\nabla\cdot\mathbf{v}=0, \tag{28}$$

$$\rho_t'+(h\mathbf{v}\cdot\nabla)\rho'=\kappa\Delta\rho'-h\mathbf{v}\cdot\nabla\overline{\rho}(z)-\rho'\nabla\cdot h\mathbf{v}, \tag{29}$$

where the first two equations are solved in the same fashion by the above-outlined projection method, and the third equation is solved using central difference discretization in spatial dimensions and Heun's predictor-corrector method for time integration.

To gain a statistical view of our numerical simulations, we eject passive tracer particles at a certain time and let the particles move according to the local fluid velocity. Numerically, to track the passive tracer particles, first we use interpolation to find the velocity field at the tracer location. Then we use a predictor-corrector method to integrate the velocity field to find the tracer location at the next time step.

In all computations to following, the grid size is 128×512. We have refined the mesh size to test the convergence of our numerical results.

V. SIMULATIONS, AND THE COMPRESSIBLE MIXING BARRIER: ZERO PRANDTL NUMBER EQUATIONS

We document phenomena directly attributable to the anelastic mass constraint, in this section for the zero-gravity anelastic system (1) and (2), then in Sec. VI for the complete anelastic system in the limit of small Prandtl number (or equivalently, large Froude number).

Specifically, we now explore *phenomena associated with structure in the mean state density profile*. We compare the evolution of the three systems: *case 1*: the incompressible system [Eqs. (1) and (2) with constant background density, $\rho(z)=1$]; then the anelastic system with two different background density profiles, *case 2*: a structureless exponential (4), and *case 3*: a transition layer (5). (Movies of the numerical simulations are available online).[17]

Figures 3–5 consist of columns 1, 2, 3 corresponding to the dynamic evolution of the vorticity field for cases 1, 2, 3 just discussed: the left column for the incompressible system, the middle column for an exponential background density (4) with scale factor $\alpha=0.02$, and the right column for a transition layer density profile (5) with parameters $\delta=4$, $\epsilon=0.1$. See Fig. 1 for the relative comparison of these two density profiles. Each output time for the three cases is approximately the same. In all simulations, the dynamic viscosity is set to 0.001, and the second viscosity is set to 0. We remark that we explored nonzero second viscosities (for values up to

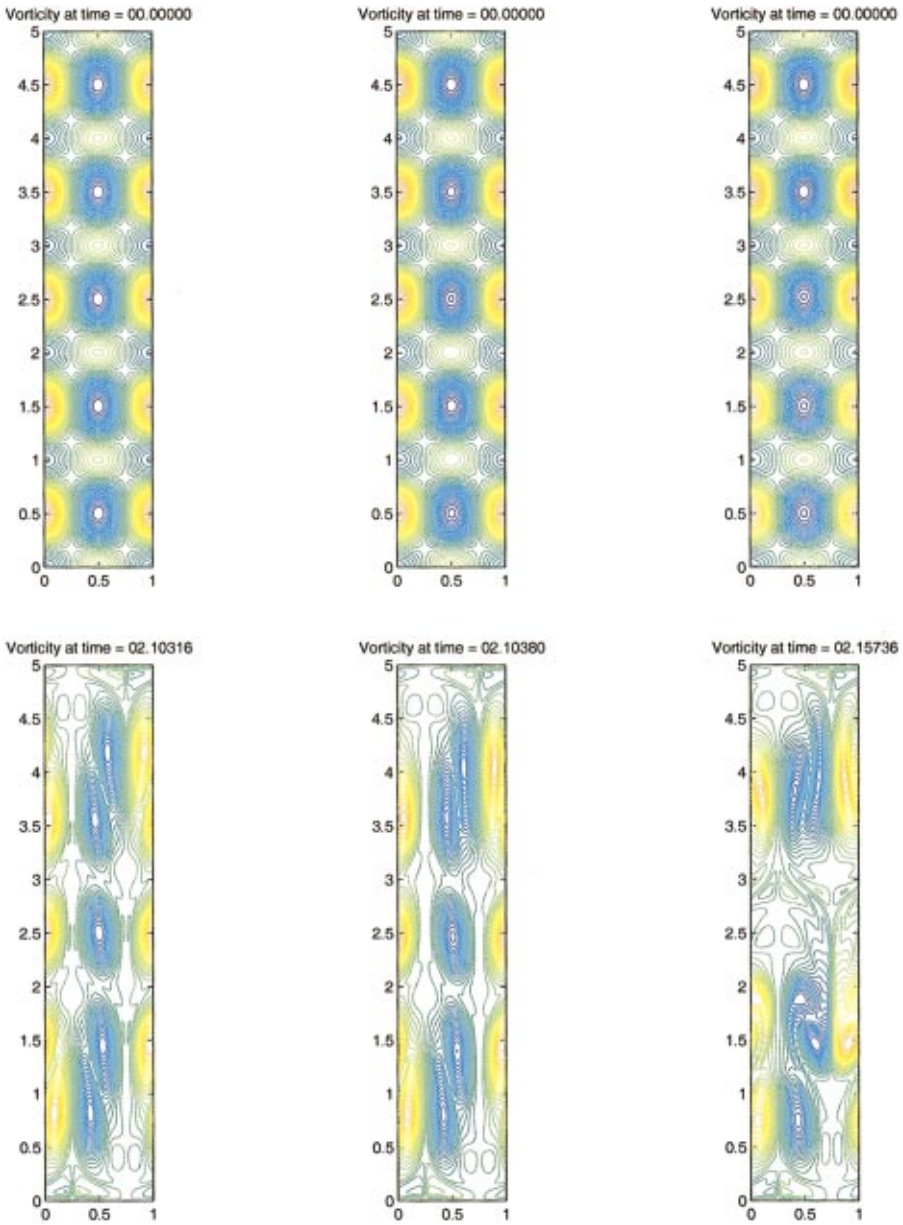

FIG. 3. (Color) Time lapses of vorticity patterns for constant density (column 1), exponential density (4) with $\alpha=0.02$ (column 2), and structured density (5) with $\delta=4$, $\epsilon=0.1$ (column 3) simulations of the anelastic model (1) and (2). In each simulation the Reynolds number is Re=1000.

0.001) and did not observe significant differences in the output. Unless otherwise noted, our channel dimensions are: $Z_L=5$, $M=1$.

We first discuss the *incompressible case, column 1*. The initial conditions selected do not represent an exact steady solution of the inviscid incompressible Euler equations, but rather are designed to produce interesting vortex interactions. The initial vorticity field is comprised of columns of vortices. Each column contains same-signed vortices, with the sign alternating periodically between columns. For the computational domain studied in this problem, five vortices are initialized in each column. Due to no-slip conditions at the walls [initially satisfied (see Eq. (6))] through the incorporation of the additional shear in the initial velocity field), like-signed vortices near the wall pair up, and propagate toward the interior. Viscosity acts to combine these vortex pairs into essentially single vortices. When these vortex blobs reach the interior, the blob above interacts with the blob below (and the central vortex appears to be absorbed in the process), producing a new, same-signed vortex pair. This vortex pair spins, and exchanges fluid from the lower half of the computational domain to the upper (and vice versa). It is precisely this fluid exchange and transport process that we explore in the ensuing anelastic simulations. We further document exchange and transport across the vertical domain through the tracking of passive tracers.

We comment that similar processes occur in each of the columns, and that this flow does not produce dynamic interaction between columns. It is an interesting question of incompressible vortex dynamics to explain the precise details of this evolution. Of course, linear stability analysis may be performed upon double arrays of point vortices. The essential mechanisms may be roughly ascertained from the comparative analysis of a single array, one with repeated same-signed, same-strength vortices, and one with alternating-signed, same-strength vortices. Clearly, these configurations

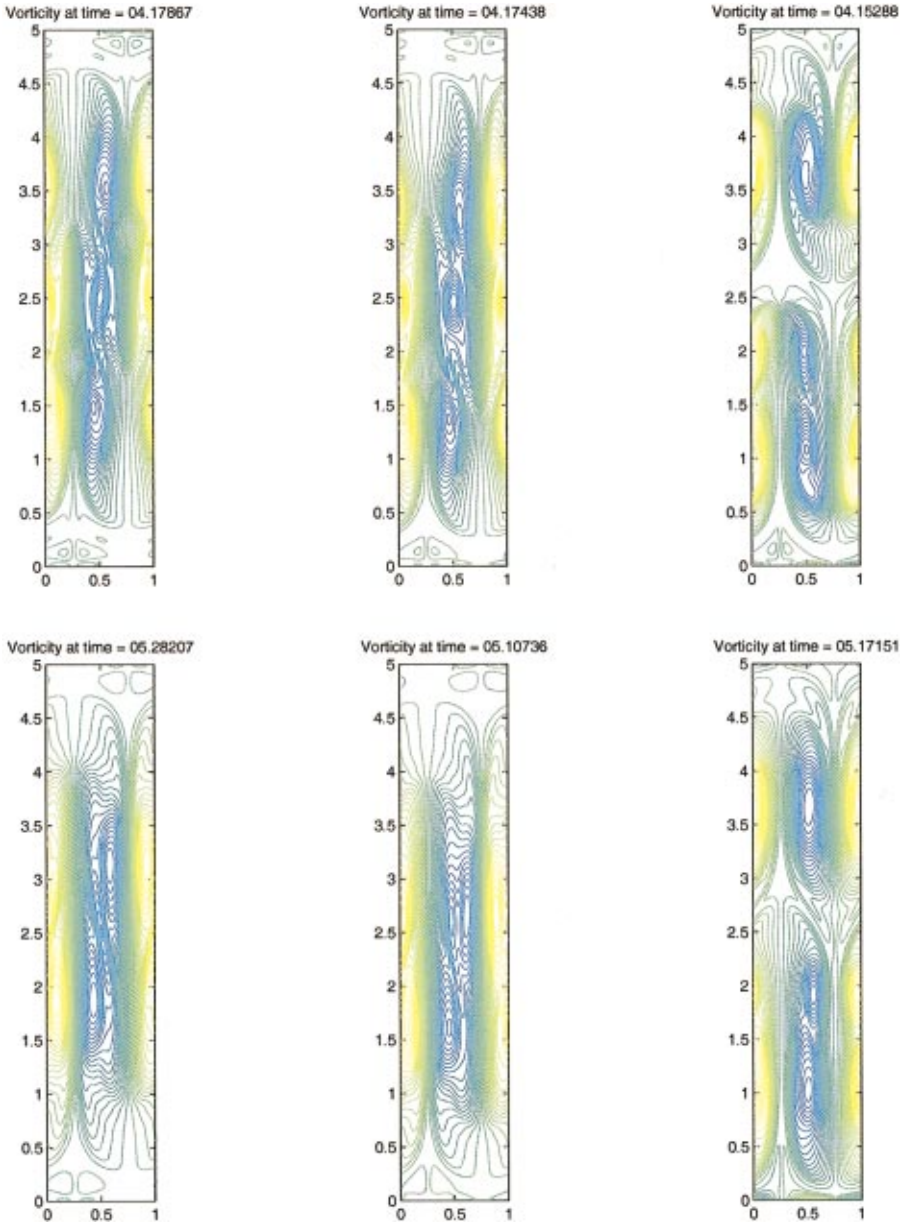

FIG. 4. (Color) Figure 3 continued.

are unstable, and it is the most unstable perturbations which suggest the initial behavior. For a same-signed array, this linear analysis suggests that neighboring vortices should pair up (as in the simulation just documented); see Saffman.[18] For the alternating array, analysis (see the Appendix) and intuition suggests that every other vortex should pair. The linearized growth rates associated with these next-nearest-neighbor pairings for the alternatingly signed array are smaller by a factor of 4 below the nearest-neighbor couplings giving maximal growth for the same-signed array. A reasonable plausibility argument to explain the vortex dynamics observed in these simulations is to conjecture that the ''perturbations'' associated with our simulations are more likely to seed the nearest-neighbor couplings, and hence the vertical, as opposed to horizontal, vortex motion observed in the simulation. Of course the calculation in the Appendix involves an infinite array, whereas the simulation involves an array of finite length.

We next discuss *column 2*, the weakly compressible simulation involving a *structureless, exponential density profile*. First, we observe overall qualitative similarity with the incompressible simulation, column 1. Same-signed vortices in the respective upper and lower domains initially pair, and subsequently merge. The process continues propagating to the interior, until the upper vortex pair meets the lower forming a single large eddy which exchanges fluid from the upper and lower domains. The one *distinguishing feature* from the incompressible simulation is the *downward shift in the stratified merger process*.

Column 3 documents the weakly compressible simulation involving a *structured background density transition layer*. Strong qualitative differences between the previous two cases are immediately evidenced through the clear formation of a vortex mixing barrier. The pairing process commences at early stages of the simulation. However, by time $t=5.1$, a strong difference is encountered. As the vortices

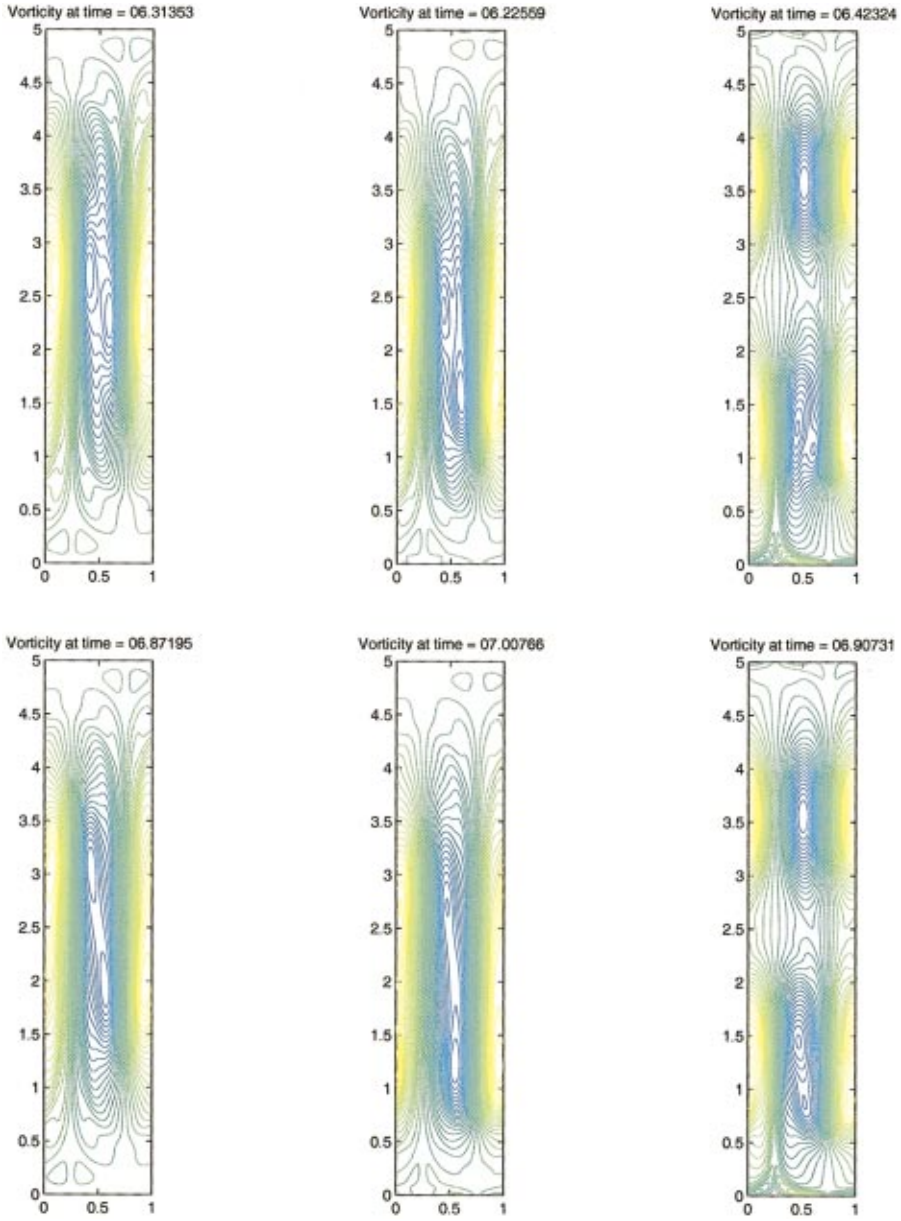

FIG. 5. (Color) Figure 4 continued.

begin to enter the region of strong density transition, the subsequent vortex merger which occurs in columns 1 and 2 *ceases*. The vortex motion is effectively blocked, and no noticeable exchange of vorticity occurs on the time scale of these simulations. On longer time scales, our simulations document that ultimately the vortices will leak through this barrier (see Fig. 9 and the discussion below). However, this time scale is difficult to describe thus far in terms of a scaling law.

To demonstrate that this simulation actually presents an effective barrier to mixing, we consider the evolution of passive markers. First, in Fig. 6 we document the velocity fields arising in Fig. 4 at time $t=4.1$. The upper field corresponds to the purely incompressible simulations, whereas the lower field is that arising from the anelastic simulation with a background transition density field. Observe the striking qualitative difference: in the weakly compressible simulation, at this output time, little fluid flows across the altitude of strong density transition. To verify that this observation is not anomalous in time, we explore tracer trajectories. At time $t=2.1$, we release 20 000 nonbuoyant, passive particles uniformly distributed over region $[0.3,0.7]\times[2.5,3.5]$ (just above the density transition) into the incompressible flow of column 1, and the anelastic transition layer flow of column 3. These particles are tracked, and we construct histograms for vertical particle distribution. Figure 7 presents these histograms for short time, and longer time. The left column presents the vertical particle distributions for the incompressible simulation, while the right column gives the analogous distribution for the anelastic simulation. Observe: at short times the distributions are similar, however at longer times, the effect of the anelastic blocking is strongly evidenced through the higher probability for finding particles above the density transition in the anelastic simulation. Clearly, the effect of strong density variation is producing an effective mixing barrier to transport in the anelastic simulation.

We lastly document how the sharpness of the transition layer lengthens the time scale for blocking in anelastic fluid

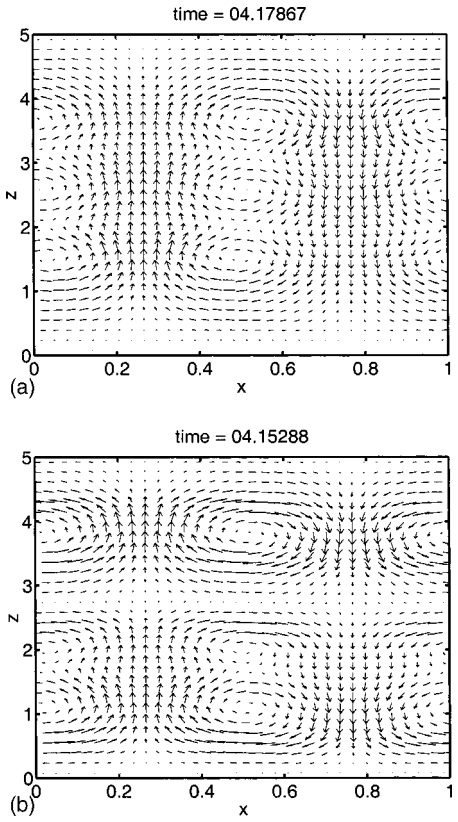

FIG. 6. The velocity field depicted in Fig. 3: (a)—top panel: corresponds to Fig. 3, column 1, whereas (b)—bottom panel—corresponds to Fig. 3, column 3.

flow. Figures 8 and 9 document the evolution for two different anelastic simulations for moderate and sharp density transition layers. The top row corresponds to a moderate density transition layer with $\delta=1$, $\epsilon=0.1$, while the bottom row corresponds to a sharper transition (of same overall density difference) with $\delta=8$, $\epsilon=0.1$. Observe that for times up to $t=4$, the qualitative vortex dynamics are similar: blocking is prevalent on these time scales. However, at longer times (shown in Fig. 9), vorticity begins to leak through the barrier for the case involving a moderate transition layer, whereas the barrier continues to block vortex exchange for the sharper density transition. This suggests a possible time scale for blocking which is dependent upon the sharpness of the density transition layer.

In closing, we further comment that length scale (for vortices, channel domain) has been studied and does not greatly alter the above-mentioned results (see website[17]).

VI. FINITE PRANDTL NUMBER SIMULATIONS

Here, we present numerical simulations of the equations in (14) for a sequence of Prandtl numbers to document that the blocking event outlined in Sec. V arises in the limit of small Prandtl number, thereby justifying the use of the zero-Prandtl number equations given in (1) and (2).

We begin with the behavior for the identical initial conditions, and geometries utilized in Sec. V, only we have augmented that system to include a density perturbation. We utilize in all simulations $g=10$, $\nu=0.001$. We begin by exploring the different behavior which occurs over a range of Prandtl numbers, with Pr=10, 1, 0.1, 0.01, using diffusivities, $\kappa=0.0001$, 0.001, 0.01, 0.1. In Fig. 10, we present an analogous series of vorticity plots at different times as those presented in Figs. 3–5, only here each column corresponds to a different Prandtl number, with the first column having

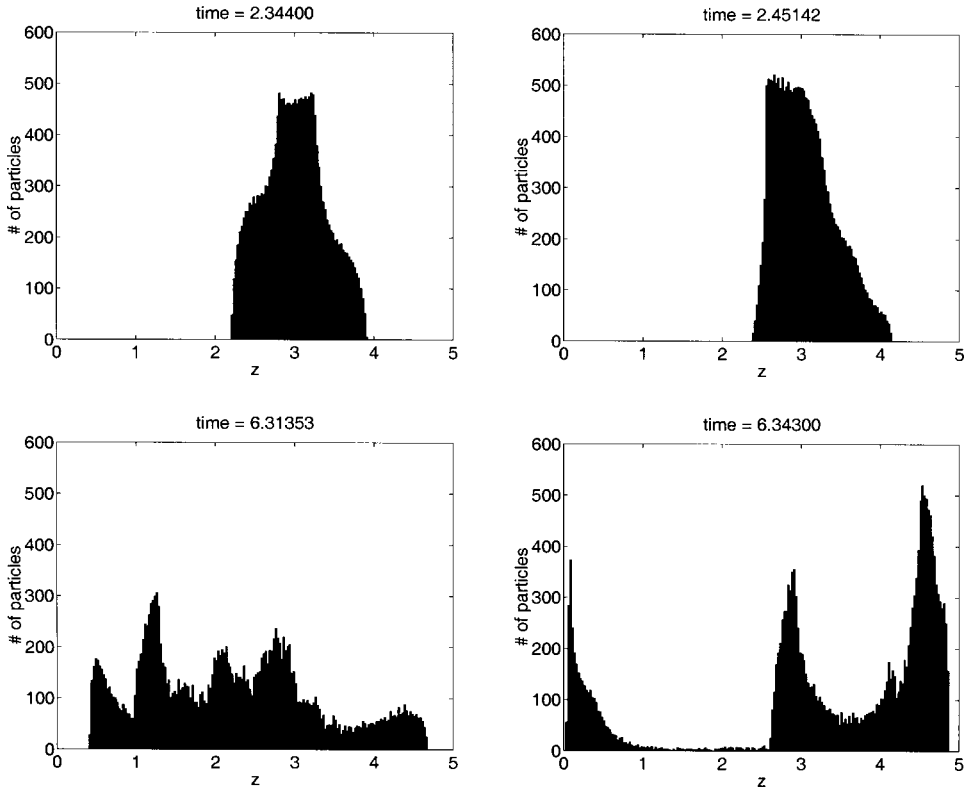

FIG. 7. The statistics of released passive scalar tracers for the simulation of Figs. 3–5: the left column is the incompressible result, while the right column is the weakly compressible result for the structured density profile.

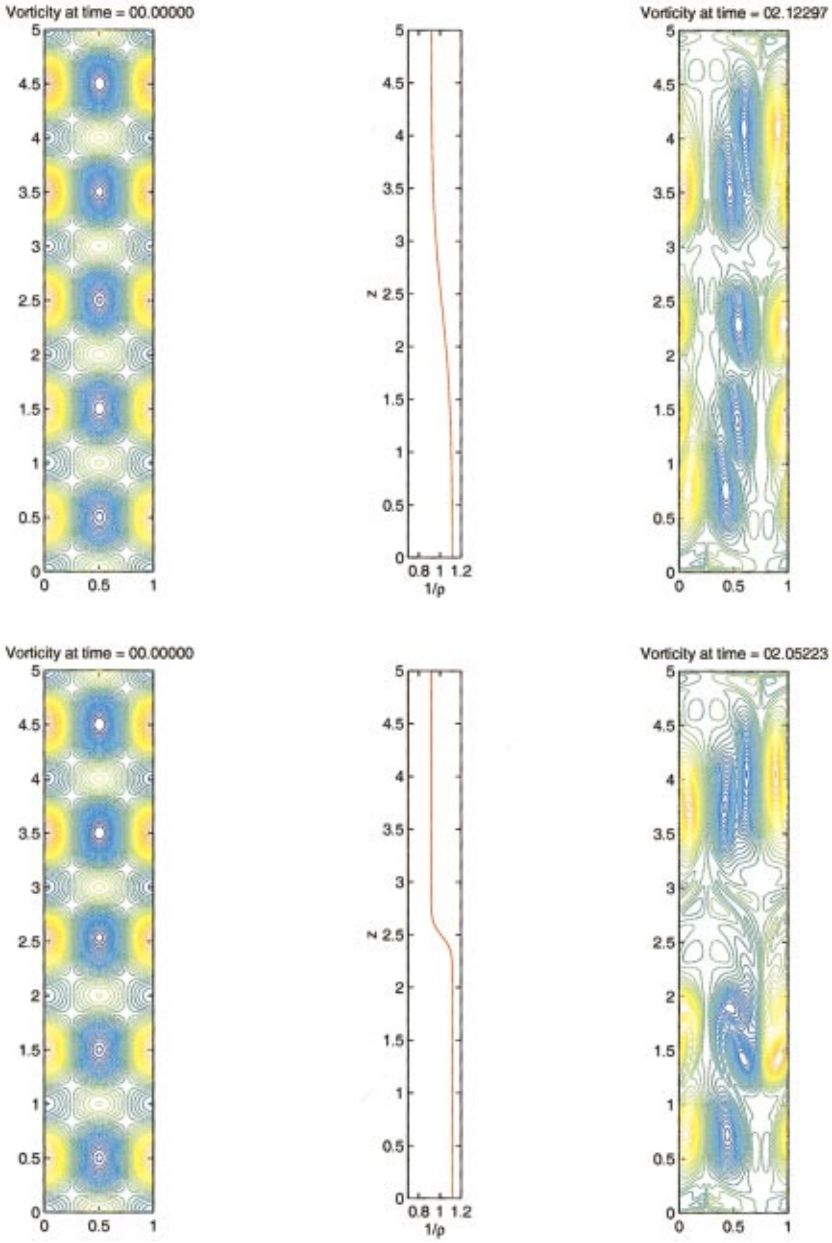

FIG. 8. (Color) A comparison of the mixing behavior of structured densities (5) as the transition width ($1/\delta$) is varied: the top simulation has $\epsilon=0.1$, $\delta=1$; whereas the lower simulation has $\epsilon=0.1$, $\delta=8$.

Pr=10, the second, Pr=1, the third, Pr=0.1, and the fourth, Pr=0.01. The trend is clear: while cases display intriguing vortex interactions, the behavior at small Prandtl number is first notably most similar to that documented by the zero-Prandtl number equations displayed in the right column of Figs. 3–5, and second, the cases with smaller Prandtl number exhibit much stronger blocking behavior than those at higher Prandtl number.

To further exemplify this trend for stronger blocking to emerge in the limit of small Prandtl number, in Fig. 11 we present particle statistics identical to those given in Fig. 7, except here, we have four columns, with Prandtl numbers akin to those in Fig. 10. The phenomena are clear as the Prandtl number is decreased: a clear wall to transport becomes apparent in the simulations with the majority of the particles remaining in the upper half of the simulation domain.

VII. CONCLUSION AND DISCUSSION

We have presented numerical simulations which document a striking weakly compressible phenomenon: *structure in the steady background density profile* during high Froude number anelastic fluid flow yields an *effective mixing barrier* which strongly modifies vortex dynamics as compared with the incompressible or structureless density counterpart. In these simulations, blocking is evidenced through particle studies which exhibit that *the anelastic fluid system has reduced mixing as compared with incompressible simulations*. The time scale for this blocking is seen to grow with the sharpness of the density transition. We additionally isolated this particular blocking event as emerging in the limit of small Prandtl number through a sequence of computational simulations of the complete anelastic system with density perturbation. As the Prandtl number was reduced, tracer his-

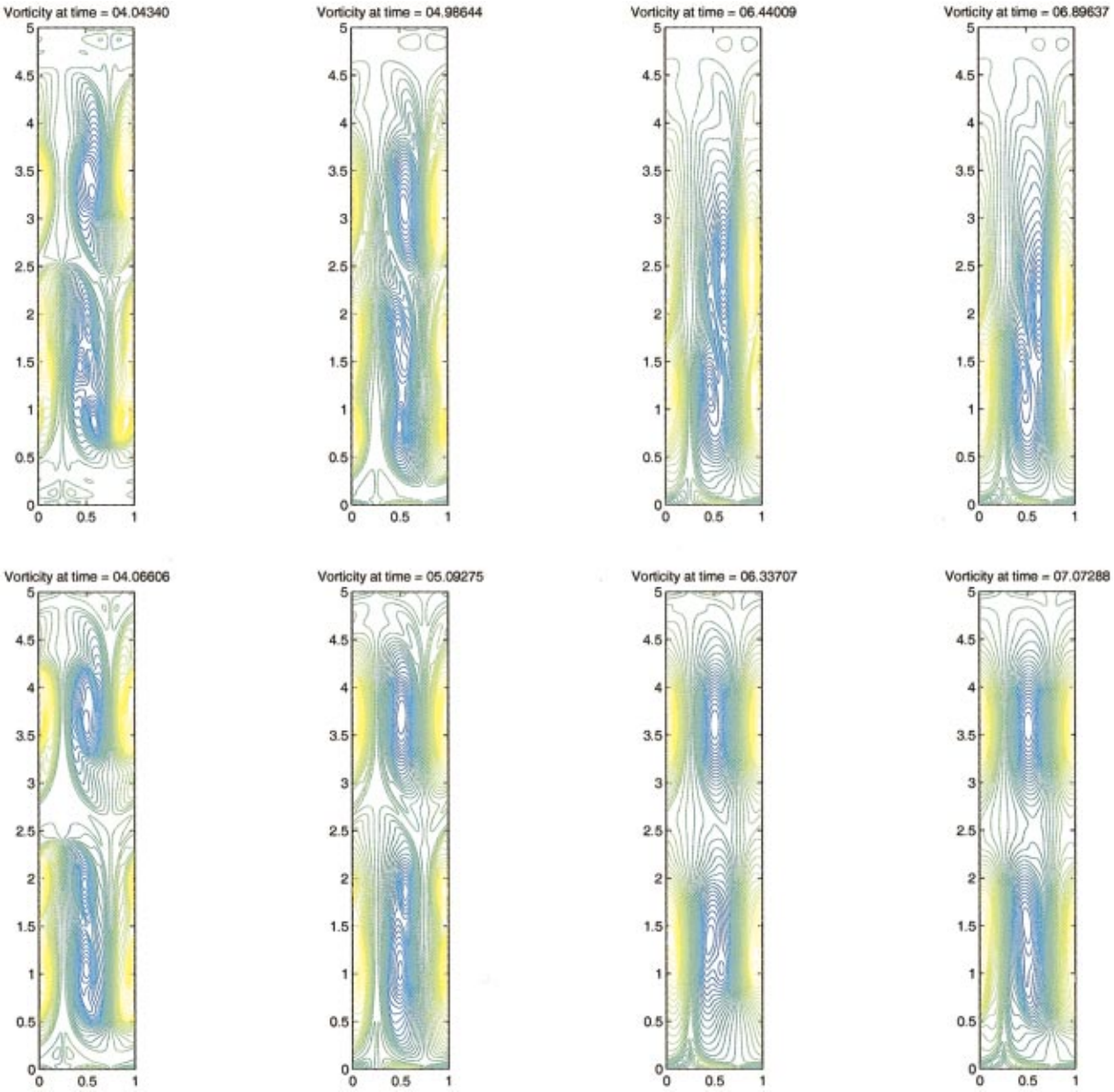

FIG. 9. (Color) Figure 8 continued, again with $\delta=1$, 8 for the upper, lower simulations, respectively.

tograms indicate a transport barrier. Consequently, this offers strong support for utilizing the zero-Prandlt number (low gravity) equations developed here, especially for flows involving such vortex interactions, for fluids with small Prandtl (or equivalently large Froude) number. Therefore, it seems natural that this blocking mechanism may be relevant to any exchange problem involving a strongly stratified fluid. Clearly, many issues need to be explored. The development of an anelastic vortex method could offer insight into the nonlinear mechanisms responsible for this mixing barrier. Work in progress has been successful in explaining certain aspects of this evolution in limiting cases, however, it is necessary to handle a variable coefficient Green's function to generalize the vortex method[19,20] to arbitrary anelastic flow.

Numerous additional issues demand consideration. Perhaps most important is a further careful assessment and understanding of the energetic scales associated with condensation and other phase change phenomena. Certainly, such phenomena are crucial to moist atmospheric convection, nonetheless, the present study does suggest that at least for dry convection non-Boussinesq effects such as those embodied within the nontrivial anelastic mass constraint yield interesting behavior associated with transport and mixing. Further, should such non-Boussinesq effects be consistently developed into closure models for driven turbulence in the presence of strong density transition? Clearly, buoyancy effects are important in the consideration of such closures, but care should be taken. Typical Richardson dependent closures often extinguish mixing coefficients for large Richardson number.[21,22] While such closures have proven effective in some circumstances, the work of Majda and Shefter has demonstrated situations in which instability persists at arbi-

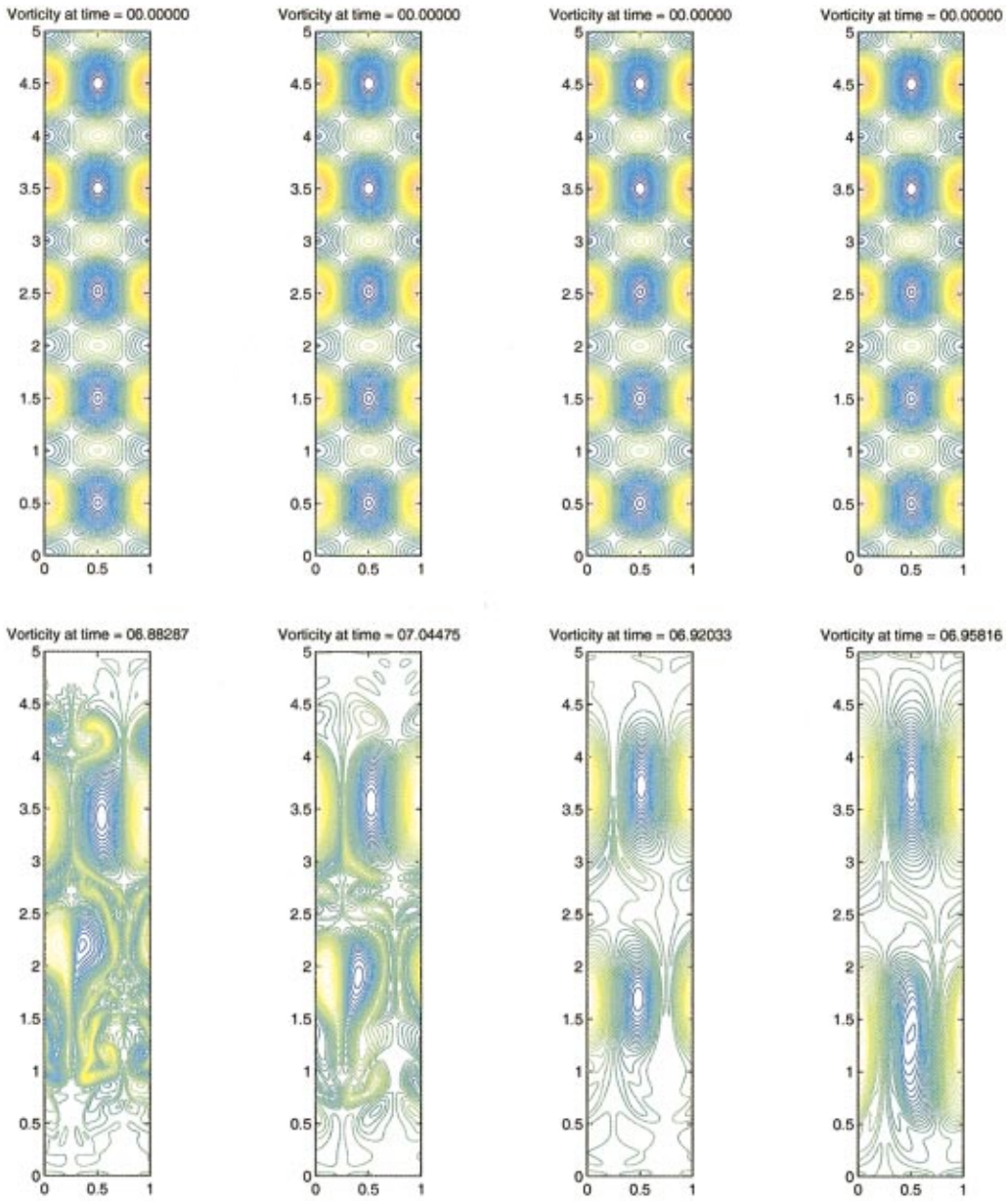

FIG. 10. (Color) Time lapses of vorticity patterns for a sequence of finite Prandtl number simulations: Pr=10 (column 1); Pr=1 (column 2); Pr=0.1 (column 3); Pr=0.01 (column 4).

trarily large Richardson number,[23] suggesting the need for modified closures. Certainly, for strong density transition, mixing should be carefully assessed as penetrative motion will experience dramatic increase in potential energy which could potentially drive smaller scale mixing upon relaxation. The studies presented here, while idealized, do suggest that mixing mechanisms may be strongly modified through weakly compressible effects, and a complete mathematical theory for small scale stratified mixing may require the consideration of such non-Boussinesq effects.

ACKNOWLEDGMENTS

M.G.F. and H.Z. are supported by the Air Force Office of Scientific Research F49620-99-1-0003, and National Science Foundation (NSF) Grant No. DMS-9704549, R.M.M. is supported through NSF Career Grant No. DMS-97019242. R.M.M. wishes to acknowledge N. O. Renno for numerous discussions regarding effects of weak compressibility. H.Z. thanks M. Minion for helpful discussions with the numerical method. All the authors thank two anonymous reviewers for their comments and suggestions which have led to a much improved study.

APPENDIX: STABILITY OF ALTERNATING PERIODIC ARRAYS

The stability of an infinite row of vortices of equal strength has been discussed in Lamb[24] and Saffman.[18] It is found that the pairing instability is most unstable for an infinite row of vortices of equal strength.

In this appendix we consider an infinite row of vortices of alternating strength. The equilibrium configuration con-

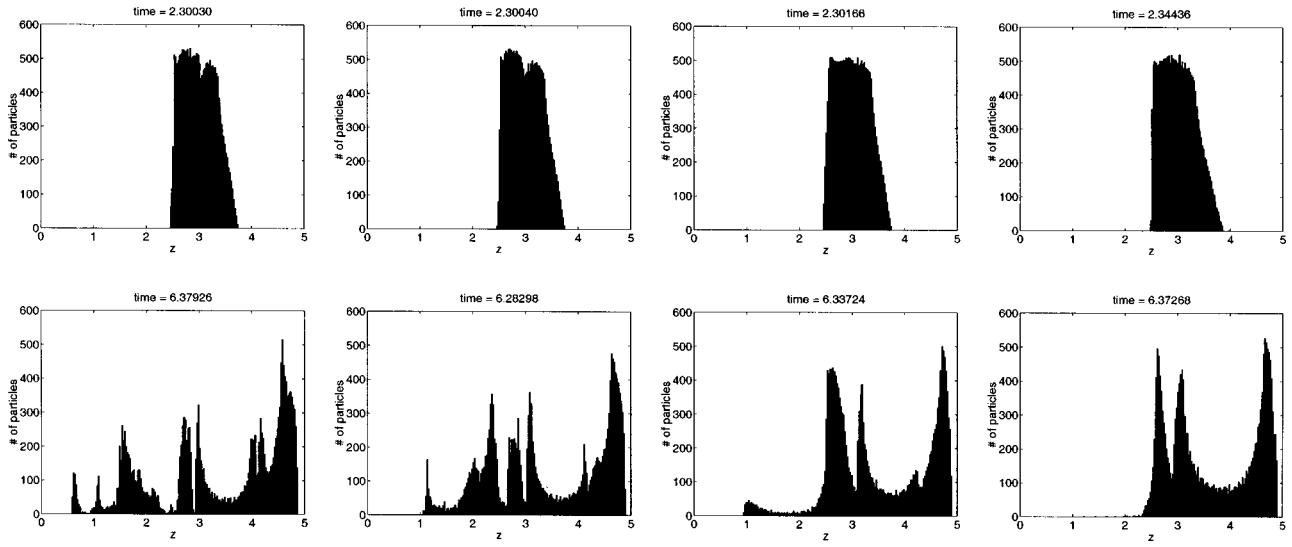

FIG. 11. The statistics of released passive scalar tracers for the simulations of Fig. 10. Viewed from the left to the right, the columns correspond to Pr=10, 1, 0.1, 0.01, respectively.

sists of vortices of strength $(-1)^k\Gamma$ at the points $x=kh$, $y=0$ $(k=-\infty,\ldots,-1,0,1,\ldots,\infty)$.

Now disturb the row

$$\mathbf{x}_j=\begin{pmatrix} hj \\ 0 \end{pmatrix}+\epsilon\mathbf{y}_j, \tag{A1}$$

where $\epsilon\ll 1$, $j=-\infty,\ldots,-1,0,1,\ldots,\infty$. Then

$$\frac{d\mathbf{x}_j}{dt}=\mathbf{J}\Gamma\sum_{k\neq j}\frac{\Gamma_k(\mathbf{x}_j-\mathbf{x}_k)}{|\mathbf{x}_j-\mathbf{x}_k|^2}, \tag{A2}$$

where

$$\Gamma_k=(-1)^k,\quad \mathbf{J}=\begin{pmatrix} 0 & -1 \\ 1 & 0 \end{pmatrix}. \tag{A3}$$

The linearized equation is

$$\frac{d\mathbf{y}_j}{dt}=\frac{\Gamma}{h^2}\mathbf{H}\sum_{k\neq j}\frac{(-1)^k(\mathbf{y}_j-\mathbf{y}_k)}{(j-k)^2}, \tag{A4}$$

where

$$\mathbf{H}=\begin{pmatrix} 0 & -1 \\ -1 & 0 \end{pmatrix}. \tag{A5}$$

This stability problem may be analyzed most simply through Fourier analysis. To this end, let

$$\mathbf{f}(x,t)=\sum_k e^{-2\pi ikx}\mathbf{y}_k(t). \tag{A6}$$

Note that $\mathbf{f}(x,t)$ is periodic with respect to x with period 1 and $\mathbf{y}_k(t)$ is given by

$$\mathbf{y}_k(t)=\int_0^1 e^{2\pi ikx}\mathbf{f}(x,t)dx. \tag{A7}$$

We further introduce

$$\mathbf{f}_0(x,t)=\sum_k e^{-2\pi i(2k)x}\mathbf{y}_{2k}(t), \tag{A8}$$

$$\mathbf{f}_1(x,t)=\sum_k e^{-2\pi i(2k+1)x}\mathbf{y}_{2k+1}(t). \tag{A9}$$

It is clear that

$$\mathbf{f}(x,t)=\mathbf{f}_0(x,t)+\mathbf{f}_1(x,t). \tag{A10}$$

It can be shown that

$$\mathbf{f}_0(x,t)=\frac{\mathbf{f}(x,t)+\mathbf{f}(x+\frac{1}{2},t)}{2}, \tag{A11}$$

$$\mathbf{f}_1(x,t)=\frac{\mathbf{f}(x,t)-\mathbf{f}(x+\frac{1}{2},t)}{2}. \tag{A12}$$

It further can be shown that

$$g(x)=\sum_{l\neq 0}\frac{(-1)^l(1-e^{2\pi ilx})}{l^2} \tag{A13}$$

is the continuous periodic extension of $g(x)=-2\pi^2x^2$ on $[-\frac{1}{2},\frac{1}{2}]$. A plot of $g(x)$ is shown in Fig. 12.

Define

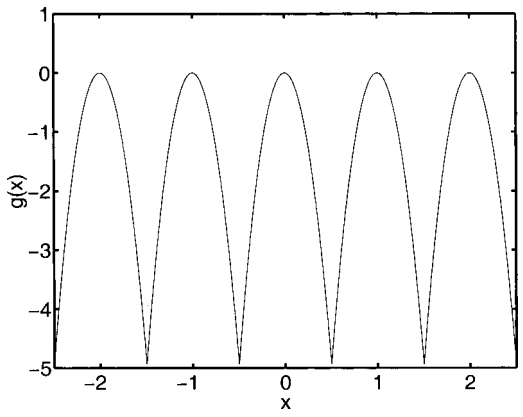

FIG. 12. The plot of $g(x)$.

$$\mathbf{f}_3 = \mathbf{f}_0 - \mathbf{f}_1 . \tag{A14}$$

Then it may be established from (A4) that

$$\frac{\partial \mathbf{f}_3}{\partial t} = \frac{\Gamma}{h^2}\mathbf{H}\mathbf{f}(x,t)g(x). \tag{A15}$$

Using (A11) and (A12), one has

$$\mathbf{f}_3 = \mathbf{f}_0 - \mathbf{f}_1 = \mathbf{f}(x+\tfrac{1}{2},t). \tag{A16}$$

From (A15), one then has

$$\frac{\partial \mathbf{f}(x+\frac{1}{2},t)}{\partial t} = \frac{\Gamma}{h^2} g(x)\mathbf{H}\mathbf{f}(x,t). \tag{A17}$$

Since (A17) is true for any x and recall from (A6) that $f(x)$ is periodic with period 1, we have

$$\frac{\partial \mathbf{f}(x,t)}{\partial t} = \frac{\partial \mathbf{f}(x+1,t)}{\partial t} = \frac{\Gamma}{h^2} g\left(x+\frac{1}{2}\right)\mathbf{H}\mathbf{f}\left(x+\frac{1}{2},t\right). \tag{A18}$$

Hence

$$\frac{\partial}{\partial t}\begin{bmatrix} \mathbf{f}(x,t) \\ \mathbf{f}\left(x+\frac{1}{2},t\right) \end{bmatrix} = \frac{\Gamma}{h^2}\begin{bmatrix} 0 & g\left(x+\frac{1}{2}\right)\mathbf{H} \\ g(x)\mathbf{H} & 0 \end{bmatrix} \times \begin{bmatrix} \mathbf{f}(x,t) \\ \mathbf{f}\left(x+\frac{1}{2},t\right) \end{bmatrix}. \tag{A19}$$

The positive eigenvalue of the matrix on the right-hand side is

$$\lambda_+ = \sqrt{g(x)g\left(x+\frac{1}{2}\right)}. \tag{A20}$$

For convenience, let us restrict x to $-\frac{1}{2} \leqslant x \leqslant 0$. Then

$$\lambda_+ = 2\pi^2 |x(x+\tfrac{1}{2})| = -2\pi^2 x(x+\tfrac{1}{2}) = 2\pi^2[-(x+\tfrac{1}{4})^2 + \tfrac{1}{16}] \tag{A21}$$

whose maximum value is $\pi^2/8$, achieved at $x = -\frac{1}{4}$. So the maximum growth rate of an infinite row of vortices of alternating strength is smaller than that of an infinite row of vortices of equal strength by a factor of 4; see Saffman.[18]

The most unstable mode is easily shown to be a pairing mechanism coupling next nearest neighbors, as opposed to the case of same signed vortices which pairs *nearest* neighbors.

[1] G. Jarvis and D. McKenzie, "Convection in a compressible fluid with infinite Prandtl number," J. Fluid Mech. **96**, 515 (1980).
[2] G. K. Batchelor, "The conditions for dynamical similarity of motions of a frictionless perfect-gas atmosphere," Q. J. R. Meteorol. Soc. **79**, 224 (1953).
[3] D. R. Durran, "Improving the anelastic approximation," J. Atmos. Sci. **46**, 1453 (1989).
[4] F. Lipps and R. Hemler, "A scale analysis of deep moist convection and some related numerical calculations," J. Atmos. Sci. **39**, 2192 (1982).
[5] Y. Ogura and N. A. Phillips, "Scale analysis of deep and shallow convection in the atmosphere," J. Atmos. Sci. **19**, 173 (1962).
[6] L. B. Nance and D. R. Durran, "A comparison of the accuracy of three anelastic systems and the pseudo-incompressible system," J. Atmos. Sci. **51**, 3549 (1994).
[7] J. Klemp, "Dynamics of tornadic thunderstorms," Annu. Rev. Fluid Mech. **19**, 369 (1987).
[8] J. M. Prusa, P. K. Smolarkiewicz, and R. R. Garcia, "Propagation and breaking at high altitudes of gravity waves excited by tropospheric forcing," J. Atmos. Sci. **53**, 2186 (1996).
[9] R. M. McLaughlin and M. G. Forest, "An anelastic scale-separated model for mixing, with application to atmospheric transport phenomena," Phys. Fluids **11**, 880 (1999).
[10] T. Elperin, N. Kleeorin, and I. Rogachevskii, "Mechanisms of formation of aerosol and gaseous inhomogeneities in the turbulent atmosphere," Atmos. Res. **53**, 117 (2000).
[11] A. S. Almgren, "A new look at the pseudo-incompressible solution to Lamb's problem of hydrostatic adjustment," J. Atmos. Sci. **57**, 995 (2000).
[12] P. R. Bannon, "On the anelastic approximation for a compressible atmosphere," J. Atmos. Sci. **53**, 3618 (1996).
[13] A. Majda and J. Sethian, "The derivation and numerical solution of the equations for zero Mach number combustion," Combust. Sci. Technol. **42**, 185 (1985).
[14] A. E. Gill, *Atmosphere-Ocean Dynamics* (Academic, New York, 1982).
[15] A. J. Chorin, "A numerical method for solving incompressible viscous flow problems," J. Comput. Phys. **135**, 118 (1997).
[16] A. Majda and A. Bertozzi, *Vorticity and Incompressible Flow* (Cambridge University Press, New York, 2001).
[17] See EPAPS Document No. E-PHFLE6-15-007310 for computational movies documenting weakly compressible transport barriers. A direct link to this document may be found in the online article's HTML reference section. The document may also be reached via the EPAPS homepage (http://www.aip.org/pubservs/epaps.html) or from ftp.aip.org in the directory /epaps/. See the EPAPS homepage for more information.
[18] P. G. Saffman, *Vortex Dynamics* (Cambridge University Press, New York, 1992).
[19] A. J. Chorin, *Mathematical Fluid Dynamics*, 3rd ed. (Springer, New York, 1993).
[20] L. Onsager, "Statistical hydrodynamics," Nuovo Cimento, Suppl. **6**, 279 (1949).
[21] J. W. Deardorff, G. E. Willis, and D. K. Lilly, "Laboratory investigation of non-steady penetrative convection," J. Fluid Mech. **35**, 7 (1969).
[22] J. Smagorinsky, "General circulation experiments with the primitive equations. I. The basic experiment," Mon. Weather Rev. **91**, 99 (1963).
[23] A. Majda and M. Shefter, "The instability of flows at large Richardson numbers," Proc. Natl. Acad. Sci. U.S.A. **95**, 7850 (1998).
[24] H. Lamb, *Hydrodynamics* (Dover, New York, 1932).